The Astrophysical Journal Letters, 928:L11 (7pp), 2022 March 20 https://doi.org/10.3847/2041-8213/ac5ccf

The Mg–K Anticorrelation in ω Centauri

Deimer Antonio Alvarez Garay[1,2], Alessio Mucciarelli[1,2], Carmela Lardo[1], Michele Bellazzini[2], and Thibault Merle[3]
[1] Dipartimento di Fisica e Astronomia, Università degli Studi di Bologna, Via Gobetti 93/2, I-40129 Bologna, Italy
[2] INAF, Osservatorio di Astrofisica e Scienza dello Spazio di Bologna, Via Gobetti 93/3, I-40129 Bologna, Italy
[3] Institut d'Astronomie et d'Astrophysique, Université Libre de Bruxelles, CP. 226, Boulevard du Triomphe, B-1050 Brussels, Belgium
Received 2022 February 14; revised 2022 March 9; accepted 2022 March 9; published 2022 March 28

Abstract

We present [K/Fe] abundance ratios for a sample of 450 stars in ω Centauri, using high-resolution spectra acquired with the multiobject spectrograph FLAMES@VLT. Abundances for Fe, Na, and Mg were also derived. We detected intrinsic K variations in the analyzed stars. Moreover, [K/Fe] shows a significant correlation with [Na/Fe] and an anticorrelation with [Mg/Fe]. The presence of a clear-cut Mg–K anticorrelation makes ω Centauri the third stellar system, after NGC 2419 and NGC 2808, hosting a subpopulation of stars with [Mg/Fe] < 0.0 dex, K-enriched in the case of ω Centauri by $\sim$0.3 dex with respect to Mg-rich stars ([Mg/Fe] > 0.0 dex). The correlation/anticorrelation between K and other light elements involved in chemical anomalies supports the idea that the spread in [K/Fe] can be associated with the same self-enrichment process typical of globular clusters. We suggest that significant variations in K abundances perhaps can be found in the most massive and/or metal-poor globular clusters as a manifestation of an extreme self-enrichment process. Theoretical models face problems explaining K production in globular clusters. Indeed, models where asymptotic giant branch stars are responsible for the Mg–K anticorrelation only qualitatively agree with the observations. Finally, we discovered a peculiar star with an extraordinary K overabundance ([K/Fe] $= +1.60$ dex) with respect to the other stars with similar [Mg/Fe]. We suggest that this K-rich star could be formed from the pure ejecta of AGB stars before dilution with pristine material.

Unified Astronomy Thesaurus concepts: Chemical abundances (224)

Supporting material: machine-readable table

1. Introduction

Over the past 30 years, increasingly accurate photometric and spectroscopic studies have changed our comprehension of the stellar populations in globular clusters (GCs). The traditional picture where all the stars in a given GC have the same age and chemical composition has been replaced by a new view where multiple populations (MPs) with different light-element abundances (C, N, O, Na, Mg, Al) are present in the same cluster (Carretta et al. 2009; Mészáros et al. 2015; Pancino et al. 2017). In contrast, GCs can still be considered chemically homogeneous with respect to heavy elements like iron and iron-peak elements, even if some GCs show variations in *s*-element abundances (e.g., Marino et al. 2015).

These chemical differences appear as correlations and anticorrelations between light elements and suggest a crucial role of the hot CNO cycle and its secondary chains Ne–Na and Mg–Al (Langer et al. 1993; Prantzos et al. 2007). The most popular theoretical models for the formation of MPs require the occurrence of subsequent episodes of star formation where second-generation stars (SG) are formed from the material polluted by stars from the first generation (FG or polluters) during the first 100–200 Myr of the cluster life.

Several stellar polluters have been proposed in the literature —intermediate-mass asymptotic giant branch (AGB) stars (D'Ercole et al. 2010), supermassive stars (Denissenkov & Hartwick 2014), fast-rotating massive stars (FRMS; Krause et al. 2013), and interacting binary stars (de Mink et al. 2009) —essentially because they are able to reach the temperatures required to activate the CNO cycle. However, all these models have difficulties accounting for all the observational evidence gathered so far (e.g., Bastian & Lardo 2018; Gratton et al. 2019). Consequently, new observational clues on the nature of the polluters are highly desirable. Potassium (K) is a new entry among elements whose abundance varies within GC stars. Mucciarelli et al. (2012) and Cohen & Kirby (2012) first discovered the presence of an extended Mg–K anticorrelation in the massive GC NGC 2419. Stars in this GC cover an unusually large range of K abundances, from solar values up to [K/Fe] $\sim +2$ dex. Magnesium also exhibits large variations, from the typical α-enhanced values observed in other GCs down to [Mg/Fe] ~ -1 dex. Such magnesium depletion has not been observed up to that time either in GCs or in the field.

The Mg–K anticorrelation was detected also in NGC 2808 (Mucciarelli et al. 2015), although less extended than that in NGC 2419. Mucciarelli et al. (2015) measured the Mg and K abundances for 12 stars of NGC 2808, and among these, 3 Mg-poor ([Mg/Fe] < 0.0 dex) stars show enhanced K abundances with respect to Mg-rich stars ([Mg/Fe] > 0.0 dex).

In NGC 4833, Carretta (2021) found evidence for intrinsic K variations in a sample of 59 stars. They also found a Mg–K anticorrelation in 38 stars, even if none of them have [Mg/Fe] < 0.0 dex.

Measured K abundances show significant correlations and anticorrelations with other light elements such as O, Na, and Al, and hence the scatter observed in [K/Fe] seems to be related to the same mechanism producing the variations in the other light elements. In particular, the Mg–K anticorrelation was detected only in very massive and/or metal-poor GCs. These would support the notion that it is a manifestation of an

extreme self-enrichment process where all the CNO secondary chains are very efficient (Mucciarelli et al. 2017).

The origin of the Mg–K anticorrelation is not clear. Ventura et al. (2012) proposed a model where the Mg-poor/K-rich stars in NGC 2419 formed from the ejecta of AGB and super-AGB stars. In their model, the consumption of Mg is accompanied not only by the production of Al but also of K from proton-capture reaction on Ar nuclei. However, in order to reproduce the abundances observed in NGC 2419, this model requires a significant increase in the reaction cross section or in the burning temperature at the base of the envelope during the hot bottom-burning (HBB) phase. On the other hand, no K production is expected in FRMS or supermassive stars, which are not able to reach the temperatures needed to synthesize K (Prantzos et al. 2017).

ω Centauri (NGC 5139) represents an interesting target to search for spread in [K/Fe]. It is one of the most complex stellar systems overall and the most massive among GCs with $M = (4.05 \pm 0.10) \times 10^6\, M_\odot$ (D'Souza & Rix 2013). It spans a large metallicity range from [Fe/H] ≈ -2.2 dex up to -0.5 dex with different peaks in the metallicity distribution (e.g., Pancino et al. 2000; Johnson & Pilachowski 2010), and it is one of the few systems hosting Mg-poor stars (Norris & Da Costa 1995; Mészáros et al. 2020). The observational properties of ω Centauri would suggest that it represents the remnant of an ancient nucleated dwarf galaxy that merged with the galaxy in early epochs (Bekki & Freeman 2003).

The large metallicity spread can be attributed to multiple star formation episodes that last a few gigayears (Smith et al. 2000; Romano et al. 2010). However, the abundances of the light elements are more similar to those observed in typical GCs than those in dwarf galaxies and include the presence of O–Na, Mg–Al, O–Al, Mg–Si anticorrelations together with Na–Al and Al–Si correlations (Norris & Da Costa 1995; Smith et al. 2000; Johnson & Pilachowski 2010; Marino et al. 2011; Pancino et al. 2017; Mészáros et al. 2020). The large metallicity distribution and the variations in light elements suggest that both core-collapse supernovae and the products of the proton-capture reactions played an important role in the ω Centauri chemical enrichment history.

Because of its complex history of formation and evolution, ω Centauri represents an ideal candidate to search for the Mg–K anticorrelation. A hint of the presence of a Mg–K anticorrelation was found by Mészáros et al. (2020). They identified seven Mg-poor stars that are slightly enriched in K compared to the Mg-rich stars in their sample. Nevertheless, the infrared lines used to derive K abundance are weak and blended, so Mészáros et al. (2020) concluded that a K enhancement in the Mg-poor stars of ω Centauri cannot be convincingly asserted.

In this study we investigate the presence of a Mg–K anticorrelation in ω Centauri. In Section 2 we present observational data and describe the analysis in Section 3. In Section 4 we review the results of the chemical analysis. Finally, we present our conclusions in Section 5.

2. Observations

Observations were performed with the multiobject spectrograph FLAMES (Pasquini et al. 2002), within the ESO program 095.D-0539 (P.I. Mucciarelli). We used FLAMES in the GIRAFFE mode that allows us to allocate simultaneously up to 132 fibers. All the targets were observed with both HR11 and HR18 setups, covering the wavelength range from 5597 to 5840 Å and from 7648 to 7889 Å, and with a spectral resolution of 29,500 and 20,150, respectively. The first setup allows us to measure the Mg line at 5711 Å and the Na doublet at 5682 and 5688 Å, the second the K I resonance line at 7699 Å. We checked, for each target, that the K line was not contaminated by telluric lines. This is due to the high radial velocity of ω Centauri (232.7 ± 0.2, $\sigma = 17.6\,\mathrm{km\,s^{-1}}$), Baumgardt & Hilker 2018). Also, several Fe lines are included in the considered wavelength range.

We selected targets among the member stars of ω Centauri already analyzed in previous works (Norris & Da Costa 1995; Johnson & Pilachowski 2010; Marino et al. 2011). Also, we considered only stars that are not contaminated by neighbor stars within the size of the GIRAFFE fibers. We observed a total of 450 stars: 350 are in common with Johnson & Pilachowski (2010), 85 with Marino et al. (2011), and 15 with Norris & Da Costa (1995).

Because the faintest targets have $V \sim 14$, two exposures of 1300 s and two of 300 s each were sufficient to reach a signal-to-noise ratio (S/N) ~ 70 and S/N ~ 100 for HR11 and HR18, respectively. The splitting of the observations allows us to get rid of the effect of cosmic rays and other spurious transient effects. During each exposure, some fibers ($\sim$15) were dedicated to observing empty sky regions to sample the sky background.

Spectra were reduced with the GIRAFFE ESO pipeline[4], which includes bias subtraction, flat-field correction, wavelength calibration, and spectral extraction. For each exposure, the individual sky spectra were median-combined together, and the resulting spectrum was subtracted from each stellar spectrum.

From visual inspection, we decided to exclude from the subsequent chemical analysis four stars (179_NDC, 201_NDC, 37024_J10, and 48099_J10) with $T_{\rm eff} < 3900$ K because their spectra were contaminated by the TiO molecular bands and one star (371_NDC) with a very low S/N with respect to other stars with similar magnitude.

3. Chemical Analysis

3.1. Atmospheric Parameters

We derived the stellar parameters from Gaia early Data Release 3 photometry (Gaia Collaboration et al. 2016, 2021). Figure 1 shows the color–magnitude diagram of ω Centauri where the position of the spectroscopic targets is marked.

Effective temperatures ($T_{\rm eff}$) were computed using the empirical $(\mathrm{BP}-\mathrm{RP})_0$–$T_{\rm eff}$ relation by Mucciarelli et al. (2021), based on the infrared flux method. The dereddened color $(\mathrm{BP}-\mathrm{RP})_0$ was obtained by assuming a color excess of $E(B-V) = 0.12 \pm 0.02$ (Harris 2010) and adopting an iterative procedure following the scheme proposed by Gaia Collaboration et al. (2018). Internal errors in $T_{\rm eff}$ due to the uncertainties in photometric data, reddening, and $(\mathrm{BP}-\mathrm{RP})_0$–$T_{\rm eff}$ relation are of the order of 85–115 K.

Surface gravities ($\log g$) were obtained from the Stefan–Boltzmann relation using the photometric $T_{\rm eff}$ and assuming a typical mass of $0.80\,M_\odot$. Luminosities were computed using the dereddened G-band magnitude with the bolometric corrections from Andrae et al. (2018) and a true distance modulus $\mathrm{DM}_0 = 13.70 \pm 0.06$ (Del Principe et al. 2006). We

[4] https://www.eso.org/sci/software/pipelines/giraffe/giraffe-pipe-recipes.html

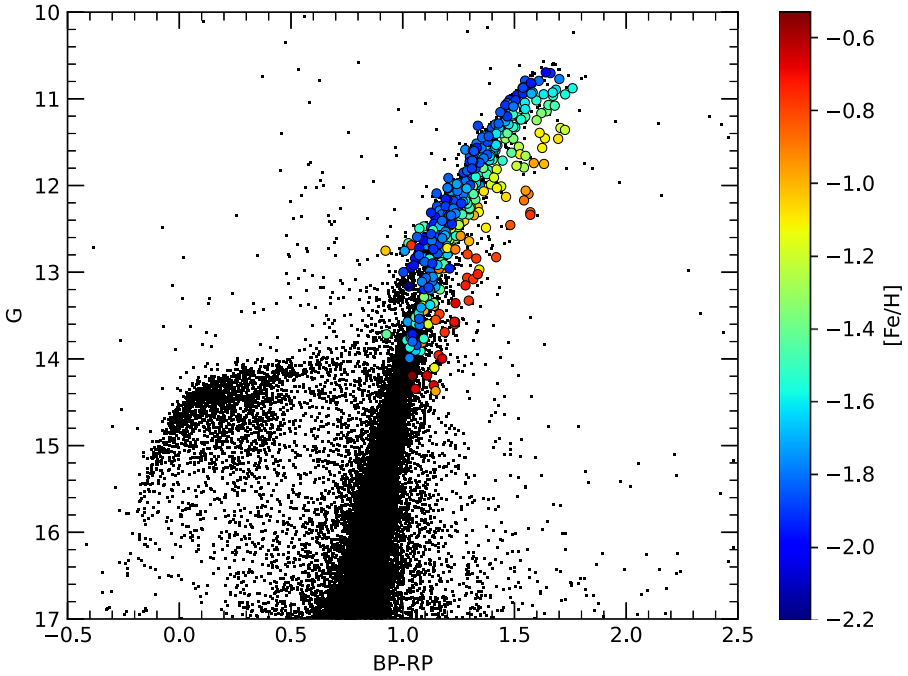

Figure 1. Color–magnitude diagram of ω Centauri. Black points represent all the targets of ω Centauri observed with Gaia, while the targets selected for this study are colored according to their metallicity. The color scale is shown on the right side.

Table 1
Data for the Analyzed Targets in ω Centauri

ID	G (mag)	v_r (km s^{-1})	$T_{\rm eff}$ (K)	log g (dex)	v_t (km s^{-1})	[Fe/H] …	[Na/Fe] …	[Mg/Fe] …	[K/Fe] …
48_NDC	10.7035	220.6	4041	0.44	2.03	-1.92 ± 0.07	-0.01 ± 0.06	0.42 ± 0.04	0.56 ± 0.15
74_NDC	11.0120	215.7	4273	0.72	1.96	-1.93 ± 0.10	0.21 ± 0.04	0.44 ± 0.03	0.41 ± 0.11
84_NDC	10.9489	220.3	3971	0.49	2.02	-1.57 ± 0.07	0.08 ± 0.09	…	0.31 ± 0.17
161_NDC	11.2326	247.3	4301	0.82	1.94	-1.74 ± 0.10	-0.26 ± 0.07	0.42 ± 0.02	0.29 ± 0.11
182_NDC	11.3292	207.3	4247	0.83	1.94	-1.53 ± 0.07	-0.06 ± 0.05	0.51 ± 0.05	0.25 ± 0.14
357_NDC	11.7420	230.9	4153	0.93	1.92	-0.97 ± 0.06	…	…	0.39 ± 0.18
480_NDC	12.2484	226.7	4503	1.35	1.82	-1.02 ± 0.11	…	…	0.48 ± 0.13
27048_J10	11.8638	242.0	4529	1.21	1.85	-1.59 ± 0.10	0.37 ± 0.06	-0.07 ± 0.05	0.53 ± 0.11
27094_J10	12.8344	237.9	4778	1.73	1.73	-1.83 ± 0.11	0.24 ± 0.06	0.44 ± 0.06	0.14 ± 0.08
29085_J10	12.3903	226.7	4730	1.53	1.78	-1.75 ± 0.10	0.21 ± 0.06	-0.37 ± 0.07	0.52 ± 0.10

Note. This is a portion of the entire table.

(This table is available in its entirety in machine-readable form.)

computed the uncertainties in gravities by propagating the uncertainties in $T_{\rm eff}$, distance modulus, and photometry. These uncertainties are of the order of 0.1 dex.

Microturbulent velocities (v_t) were obtained by adopting the relation between v_t and log g by Kirby et al. (2009). This relation provides values of v_t of about 1.6–2.0 km s^{-1}. To compute the uncertainties in v_t, we assumed a conservative error of 0.2 km s^{-1}.

The derived atmospheric parameters for all the analyzed targets are listed in Table 1, together with some additional information.

3.2. Line Lists and Tools

The chemical analysis was performed using one-dimensional, local thermodynamic equilibrium (LTE), plane-parallel geometry model atmospheres computed with the code ATLAS9 (Castelli & Kurucz 2003) that treats the line opacity through the opacity distribution functions (ODF) method. All the models are calculated using the ODFs computed by Castelli & Kurucz (2003) with α-enhanced chemical composition and without the inclusion of the approximate overshooting in the calculation of the convective flux.

A line list of relatively strong and unblended spectral features at the resolution of our GIRAFFE observations was selected from the Kurucz/Castelli line lists[5] by comparing observed spectra with synthetic ones having appropriate metallicity and $T_{\rm eff}$. Model spectra were calculated with the SYNTHE code in its Linux version (Sbordone et al. 2004; Kurucz 2005).

We derived the chemical abundances of Fe, Na, Mg, and K from the comparison between measured and theoretical equivalent widths (EWs) with the package GALA (Mucciarelli et al. 2013). EWs were measured with the code DAOSPEC

[5] https://wwwuser.oats.inaf.it/castelli/linelists.html

(Stetson & Pancino 2008) through the wrapper 4DAO (Mucciarelli 2013).

Non-LTE (NLTE) corrections for Na (at 5682 and 5688 Å) and K (at 7699 Å) were calculated by interpolating into the grids of Lind et al. (2011) and Reggiani et al. (2019), respectively.

Solar abundances are from Grevesse & Sauval (1998).

3.3. Error Estimates

Uncertainties associated with the chemical abundances were calculated as the sum in quadrature of the error related to the measurement process and the errors associated with the atmospheric parameters.[6]

The error related to the measurement was calculated as the line-to-line scatter divided by the square root of the number of lines used. When only one line was present, the error was calculated by varying the EW of $1\sigma_{\rm EW}$ (i.e., the EW error provided by DAOSPEC).

Errors related to the adopted atmospheric parameters were calculated by varying only one parameter at a time, keeping the others fixed to their best value, and recalculating the chemical abundances each time. At the end, all the error sources are added in quadrature. This approach is the most conservative in the calculation of uncertainties because it does not take into account the correlation terms between parameters. So, it should be regarded as an upper limit to the real error associated with the measurements.

Because the abundances are expressed as abundance ratios, the total uncertainties in [Fe/H] and [X/Fe] are calculated as follows:

$$\sigma_{\rm [Fe/H]} = \sqrt{\frac{\sigma^2_{\rm Fe}}{N_{\rm Fe}} + (\delta^{T_{\rm eff}}_{\rm Fe})^2 + (\delta^{\log g}_{\rm Fe})^2 + (\delta^{v_t}_{\rm Fe})^2}\,, \quad (1)$$

$$\sigma_{\rm [X/Fe]} = \sqrt{\frac{\sigma^2_{\rm X}}{N_{\rm X}} + \frac{\sigma^2_{\rm Fe}}{N_{\rm Fe}} + (\delta^{T_{\rm eff}}_{\rm X} - \delta^{T_{\rm eff}}_{\rm Fe})^2 + (\delta^{\log g}_{\rm X} - \delta^{\log g}_{\rm Fe})^2 + (\delta^{v_t}_{\rm X} - \delta^{v_t}_{\rm Fe})^2}\,, \quad (2)$$

where $\sigma_{\rm X,Fe}$ is the line-to-line scatter, $N_{\rm X,Fe}$ the number of lines used to compute the abundance, and $\delta^{i}_{\rm X,Fe}$ are the abundance variations obtained after varying the atmospheric parameter i.

4. Results

4.1. Mg–K Anticorrelation

Potassium elemental abundances were derived for a total of 440 stars. Moreover, we obtained Fe, Na, and Mg abundances for 440, 359, and 357 stars, respectively (Table 1).

The mean value of the [K/Fe] distribution is +0.31 dex ($\sigma = 0.19$ dex), with values ranging from −0.20 dex up to +0.94 dex. In this calculation we excluded one star showing a significantly higher [K/Fe] and which we will discuss in Section 4.2.

The main result of our study is the presence of a clear anticorrelation between [Mg/Fe] and [K/Fe] shown in the left-hand panel of Figure 2. We identified a sample of stars with [Mg/Fe] < 0.0 dex that are systematically enriched in [K/Fe]. These kinds of stars are rarely observed in GCs.

Also, K correlates with Na (see the right-hand panel of Figure 2). To quantitatively assess these results, we computed for the couples [K/Fe]–[X/Fe] (with X = Na and Mg) the Spearman's correlation coefficient (C_S) and the corresponding two-tailed probability that an absolute value C_S larger than the observed one can be derived from noncorrelated random variables. We found $C_S = +0.41$ and -0.52 for [K/Fe]–[X/Fe] (with X = Na and Mg), respectively, leading to a null probability that the observed correlations arose by chance from uncorrelated variables.

A hint of the presence of a Mg–K anticorrelation in ω Centauri was first detected by Mészáros et al. (2020). They found seven stars with [Mg/Fe] < 0.0 dex (out of a total sample of 898 stars) in which [K/Fe] seems to be enhanced with respect to stars with [Mg/Fe] > 0.0 dex (see their Figure 10). Unfortunately, the K lines in *H* band measured by Mészáros et al. (2020) are weak and blended with other lines. Therefore, the authors concluded that it is not possible to claim convincingly the presence of a K enhancement in the Mg-poor stars of ω Centauri. Hence, this is the first time that the presence of a strong Mg–K anticorrelation is undoubtedly established in ω Centauri.

4.2. A Super K-rich Star

In the analyzed sample, we identified a peculiar star, named 43241_J10, that clearly stands out from the mean locus of other ω Centauri members in the [Mg/Fe] versus [K/Fe] distribution, as can be seen in the left-hand panel of Figure 3. Indeed, this star has [K/Fe] = +1.60 dex.

We compared its spectrum with that of a reference star (41375_J10), with similar atmospheric parameters and [Fe/H] and [Mg/Fe] abundance ratios. In the right-hand panel of Figure 3, the observed K lines of the two stars are directly compared, showing the obvious difference in line depth, implying an intrinsic difference in the [K/Fe] abundance.

This star was also included in the sample studied by Johnson & Pilachowski (2010). For stars in common between the two studies, we found that our temperatures are on average (140 ± 94 K) higher than those computed by Johnson & Pilachowski (2010). Thus, the difference of +185 K computed for 43241_J10 in this study with respect to Johnson & Pilachowski (2010) is well within the mean difference between the two temperature scales. Even if we adopt the temperatures by Johnson & Pilachowski (2010), the difference in K abundance of 43241_J10 with respect to the other stars remains.

Therefore, we can conclude that the high-[K/Fe] abundance of this star is real and not an artifact of the analysis.

5. Discussion

Our analysis of a large sample of 450 giants in ω Centauri has revealed the presence of (1) a large intrinsic spread in the [K/Fe] and (2) a correlation between the K abundances and other light elements (i.e., Na and Mg), which are observed to vary in GCs showing MPs. In particular, we detected the presence of a prominent Mg–K anticorrelation. This finding makes ω Centauri the third stellar system after NGC 2419 (Mucciarelli et al. 2012 and Cohen & Kirby 2012) and NGC 2808 (Mucciarelli et al. 2015) in which a subpopulation of stars with [Mg/Fe] < 0.0 dex and enriched in K is present (Figure 4).

[6] If we add in quadrature all the possible sources of errors, the uncertainties would increase from a minimum of 0.02 for Na to a maximum of 0.06 dex for K, which is the most problematic element to measure. However, the results of our study are the same even if we adopt this extremely conservative approach to estimate errors.

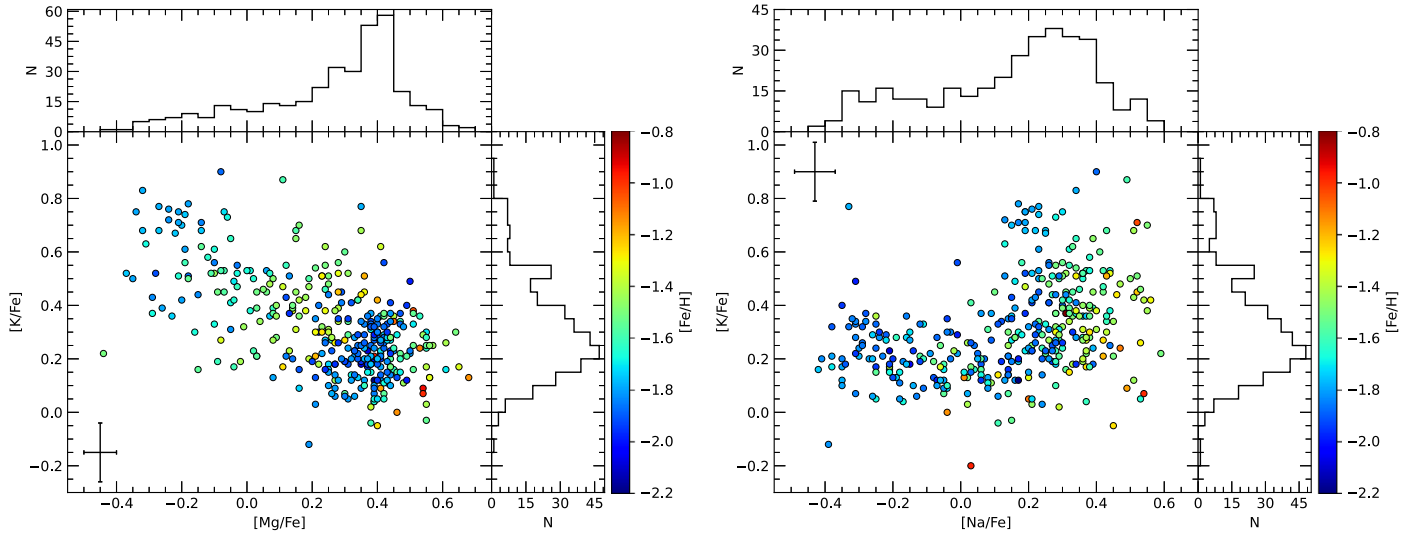

Figure 2. Left panel: behavior of [K/Fe] as a function of [Mg/Fe]. Each star is color coded according to its value of [Fe/H], and the color scale is shown on the right side. The error bar represents the typical error associated with the abundance ratios. The distribution of [K/Fe] and [Mg/Fe] are shown as marginalized histograms. Right panel: the same as the left panel, but for the [K/Fe] and [Na/Fe] abundance ratios.

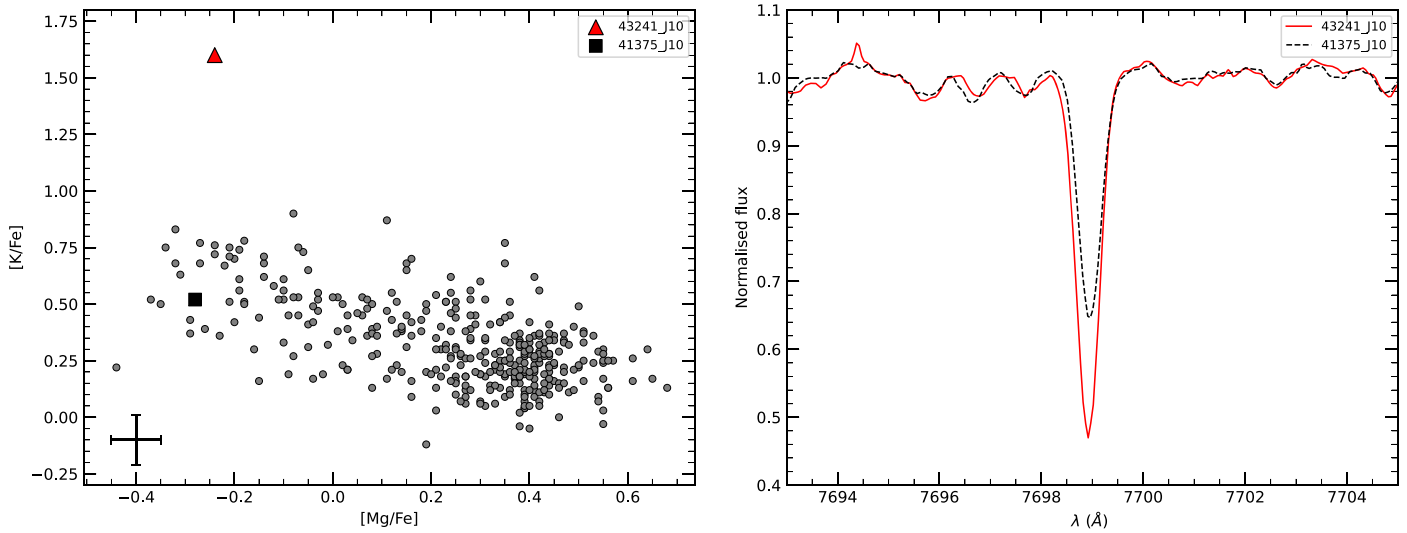

Figure 3. Left panel: behavior of [K/Fe] as a function of [Mg/Fe] with the inclusion of the K-rich star 43241_J10 (red triangle). The black square represents the reference star 41375_J10 with similar atmospheric parameters to the K-rich star. Right panel: comparison between the GIRAFFE spectra of the two stars around the strong K line at 7699 Å. The large K enhancement of 43241_J10 is clearly visible from this comparison.

The amplitude of the [K/Fe] spread in ω Centauri is intermediate between that of NGC 2419 and NGC 2808. Carretta (2021) suggested the presence of a weak (but statistically significant) Mg–K anticorrelation in NGC 4833. In this cluster the stars showing the highest Mg depletion exhibit a typical overabundance in K of 0.1 dex with respect to the most Mg-rich stars. However, this cluster does not harbor stars with [Mg/Fe] < 0.0 dex at variance with NGC 2419, NGC 2808, and ω Centauri.

The chemical complexity of the stellar populations of ω Centauri deserves further discussion of the measured [K/Fe] abundance ratios and their correlations with other light elements for the different groups of stars with distinct metallicities. The extent of the Mg–K anticorrelation is mainly driven by the metal-poor ([Fe/H] $\leqslant -1.70$ dex) component, which exhibits a bimodal distribution both in [K/Fe] and in [Mg/Fe]. In particular, the group of metal-poor stars with [Mg/Fe] < 0.0 dex has a mean value of [K/Fe] $\sim$0.4 dex higher than that of the Mg-rich, metal-poor stars. On the other hand, an evident but less extended Mg–K anticorrelation is also detected among the stars with intermediate [Fe/H] ($-1.70 <$ [Fe/H $\leqslant -1.30$ dex]). Finally, for the most metal-rich population ([Fe/H] > -1.30 dex), we cannot conclude for the presence of a Mg–K anticorrelation. For this group of stars, we do not have objects with [Mg/Fe] < 0.0 dex, and the spread in [K/Fe] is less extended than that of the other subpopulations.

The evidence of a correlation between K and the other light elements involved in the MP phenomenon supports the idea that the spread in [K/Fe] can be ascribed to the self-enrichment process typical of GCs.

The detection of an intrinsic variation in K abundances in the most massive clusters represents a serious challenge for theoretical models of the MPs. In the model proposed by Ventura et al. (2012) to explain the Mg–K anticorrelation in

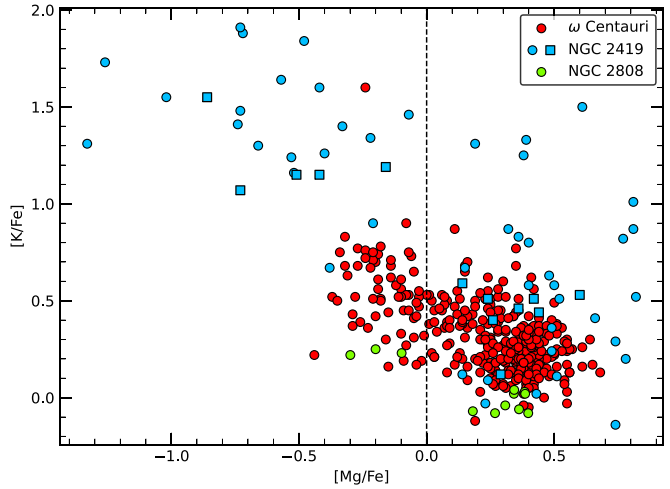

Figure 4. Run of the [K/Fe] abundance against [Mg/Fe] for stars in GCs. ω Centauri stars are shown as red circles. Stars in NGC 2808 are plotted as green circles (Mucciarelli et al. 2015), whereas stars in NGC 2419 are in blue (data from Mucciarelli et al. (2012) and Cohen & Kirby (2012) are shown as circles and squares, respectively). The dashed line splits the Mg-poor from the Mg-rich stars.

NGC 2419 and based on AGB and super-AGB stars, the production of K occurs during the HBB phase by proton-capture reaction on argon nuclei at temperatures $T \sim 10^8$ K. Even if the AGB yields discussed by Ventura et al. (2012) are qualitatively able to explain a Mg–K anticorrelation, the observed [K/Fe] abundance ratios in the extreme case of NGC 2419 can be reproduced only with an increase (1) in the cross section of the reaction ^{38}Ar(p, γ)^{39}K by a factor 100 with respect to literature or (2) in the temperature at the base of the envelope up to 1.5×10^8 K during the HBB. Moreover, Ventura et al. (2012) also predicted that Mg-poor stars would show normal Na abundances if the Mg–K anticorrelation was indeed produced by AGB and super-AGB stars. This is not observed in ω Centauri, where the Mg-poor stars are also enhanced in Na.

On the other hand, Prantzos et al. (2017) discuss the possible production of K from FRMS and supermassive stars, ruling out both classes of polluters because they are not able to reach the temperature of K burning. Therefore, the existence of MPs in GCs remains largely unexplained.

Another interesting result that we found is the presence of a peculiar star with a [K/Fe] $\sim$ 1 dex higher than the abundances of Mg-poor, metal-poor stars. Even if the origin of this extraordinary overabundance of [K/Fe] is unclear, it is worth noting that the Mg and K abundances of this star are very similar to those of NGC 2419 (see Figure 4) for which Ventura et al. (2012) proposed that the K-enhanced subpopulation was born from the AGB and super-AGB ejecta without a dilution process.

The metal-poor population of ω Centauri exhibits the usual light-element anticorrelations typical of GCs with MPs. Assuming a scenario where the K enhancement in Mg-poor stars is due to pollution by the first generation of AGB and super-AGB stars, the ejected gas undergoes a dilution process with the pristine GC gas before forming new generations of stars (D'Ercole et al. 2008, 2010). In this scenario, it is possible that a small fraction of stars will form directly from the ejecta of polluters without being diluted by pristine material. In this framework, we can suppose that the super K-rich star we discovered formed directly from the pure ejecta of AGB stars before dilution, while the other Mg-poor stars show a lower [K/Fe] due to a level of dilution with pristine material. Further inspections of this star are necessary to understand its origin. In particular, it would be useful to study other light elements involved in proton-capture reactions (C, N, O, etc).

In conclusion, with the present analysis, we support the idea that the observed spread in [K/Fe] in ω Centauri stars is associated with a self-enrichment process typical of GCs. So far, a clear Mg–K anticorrelation was found only in three GCs, namely ω Centauri, NGC 2808, and NGC 2419. Those clusters are among the most massive stellar systems of the Milky Way, so we suggest that this anomaly is a manifestation of an extreme self-enrichment process that occurs only in the most massive and/or metal-poor clusters.

C.L. acknowledges funding from Ministero dell'Università e della Ricerca (MIUR) through the Programme Rita Levi Montalcini (grant PGR18YRML1).

ORCID iDs

Deimer Antonio Alvarez Garay https://orcid.org/0000-0002-9156-0729
Alessio Mucciarelli https://orcid.org/0000-0001-9158-8580
Carmela Lardo https://orcid.org/0000-0002-4295-8773
Michele Bellazzini https://orcid.org/0000-0001-8200-810X
Thibault Merle https://orcid.org/0000-0001-8253-1603

References

Andrae, R., Fouesneau, M., Creevey, O., et al. 2018, A&A, 616, A8
Bastian, N., & Lardo, C. 2018, ARA&A, 56, 83
Baumgardt, H., & Hilker, M. 2018, MNRAS, 478, 1520
Bekki, K., & Freeman, K. C. 2003, MNRAS, 346, L11
Carretta, E. 2021, A&A, 649, 154
Carretta, E., Bragaglia, A., Gratton, R. G., et al. 2009, A&A, 505, 117
Castelli, F., & Kurucz, R. L. 2003, in Proceedings of the 210th Symposium of the IAU, Modelling of Stellar Atmospheres, ed. N. Piskunov, W. W. Weiss, & D. F. Gray (San Francisco, CA: PASP)
Cohen, J. G., & Kirby, E. N. 2012, ApJ, 760, 86
de Mink, S. E., Pols, O. R., Langer, N., & Izzard, R. G. 2009, A&A, 507, L1
Del Principe, M., Piersimoni, A. M., Storm, J., et al. 2006, ApJ, 652, 362
Denissenkov, P. A., & Hartwick, F. D. A. 2014, MNRAS, 437, L21
D'Ercole, A., D'Antona, F., Ventura, P., Vesperini, E., & McMillan, S. L. W. 2010, MNRAS, 407, 854
D'Ercole, A., Vesperini, E., D'Antona, F., McMillan, S. L. W., & Recchi, S. 2008, MNRAS, 391, 825
D'Souza, R., & Rix, H.-W. 2013, MNRAS, 429, 1887
Gaia Collaboration, Babusiaux, C., van Leeuwen, F., et al. 2018, A&A, 616, A10
Gaia Collaboration, Brown, A. G. A., Vallenari, A., et al. 2021, A&A, 649, A1
Gaia Collaboration, Prusti, T., de Bruijne, J. H. J., et al. 2016, A&A, 595, A1
Gratton, R., Bragaglia, A., Carretta, E., et al. 2019, A&ARv, 27, 8
Grevesse, N., & Sauval, A. J. 1998, SSRv, 85, 161
Harris, W. E. 2010, arXiv:1012.3224
Johnson, C. I., & Pilachowski, C. A. 2010, ApJ, 722, 1373
Kirby, E. N., Guhathakurta, P., Bolte, M., Sneden, C., & Geha, M. C. 2009, ApJ, 705, 328
Krause, M., Charbonnel, C., Decressin, T., Meynet, G., & Prantzos, N. 2013, A&A, 552, A121
Kurucz, R. L. 2005, MSAIS, 8, 14
Langer, G. E., Hoffman, R., & Sneden, C. 1993, PASP, 105, 301
Lind, K., Asplund, M., Barklem, P. S., & Belyaev, A. K. 2011, A&A, 528, A103
Marino, A. F., Milone, A. P., Karakas, A. I., et al. 2015, MNRAS, 450, 815
Marino, A. F., Milone, A. P., Piotto, G., et al. 2011, ApJ, 731, 64
Mészáros, S., Martell, S. L., Shetrone, M., et al. 2015, AJ, 149, 153
Mészáros, S., Masseron, T., García-Hernández, D. A., et al. 2020, MNRAS, 492, 1641

Mucciarelli, A. 2013, arXiv:1311.1403
Mucciarelli, A., Bellazzini, M., Ibata, R., et al. 2012, MNRAS, 426, 2889
Mucciarelli, A., Bellazzini, M., & Massari, D. 2021, A&A, 653, A90
Mucciarelli, A., Bellazzini, M., Merle, T., et al. 2015, ApJ, 801, 68
Mucciarelli, A., Merle, T., & Bellazzini, M. 2017, A&A, 600, A104
Mucciarelli, A., Pancino, E., Lovisi, L., Ferraro, F. R., & Lapenna, E. 2013, ApJ, 766, 78
Norris, J. E., & Da Costa, G. S. 1995, ApJ, 447, 680
Pancino, E., Ferraro, F. R., Bellazzini, M., Piotto, G., & Zoccali, M. 2000, ApJL, 534, L83
Pancino, E., Romano, D., Tang, B., et al. 2017, A&A, 601, A112
Pasquini, L., Avila, G., Blecha, A., et al. 2002, Msngr, 110, 1
Prantzos, N., Charbonnel, C., & Iliadis, C. 2007, A&A, 470, 179
Prantzos, N., Charbonnel, C., & Iliadis, C. 2017, A&A, 608, A28
Reggiani, H., Amarsi, A. M., Lind, K., et al. 2019, A&A, 627, A177
Romano, D., Tosi, M., Cignoni, M., et al. 2010, MNRAS, 401, 2490
Sbordone, L., Bonifacio, P., Castelli, F., & Kurucz, R. L. 2004, MSAIS, 5, 93
Smith, V. V., Suntzeff, N. B., Cunha, K., et al. 2000, AJ, 119, 1239
Stetson, P. B., & Pancino, E. 2008, PASP, 120, 1332
Ventura, P., D'Antona, F., Di Criscienzo, M., et al. 2012, ApJL, 761, L30